Vision Research 218 (2024) 108398

Contents lists available at ScienceDirect

Vision Research

journal homepage: www.elsevier.com/locate/visres

In primary visual cortex fMRI responses to chromatic and achromatic stimuli are interdependent and predict contrast detection thresholds

Rebecca Lowndes [a,b,*], Richard Aveyard [b], Lauren E. Welbourne [a,b], Alex Wade [a,b,c], Antony B. Morland [a,b,c]

[a] Department of Psychology, University of York, United Kingdom
[b] York Neuroimaging Centre, University of York, United Kingdom
[c] York Biomedical Research Institute, University of York, United Kingdom

ARTICLE INFO

Keywords:
fMRI
Primary Visual cortex
Chromatic vision
Achromatic vision
Modelling
Interdependence

ABSTRACT

Chromatic and achromatic signals in primary visual cortex have historically been considered independent of each other but have since shown evidence of interdependence. Here, we investigated the combination of two components of a stimulus; an achromatic dynamically changing check background and a chromatic (L-M or S cone) target grating. We found that combinations of chromatic and achromatic signals in primary visual cortex were interdependent, with the dynamic range of responses to chromatic contrast decreasing as achromatic contrast increased. A contrast detection threshold study also revealed interdependence of background and target, with increasing chromatic contrast detection thresholds as achromatic background contrast increased. A model that incorporated a normalising effect of achromatic contrast on chromatic responses, but not vice versa, best predicted our V1 data as well as behavioural thresholds. Further along the visual hierarchy, the dynamic range of chromatic responses was maintained when compared to achromatic responses, which became increasingly compressive.

1. Introduction

Normal human colour vision is trichromatic with three different cone classes tuned to different wavelengths in the visual spectrum (Bowmaker & Dartnall, 1980; Brown & Wald, 1964). The three cone photoreceptors are referred to as L, tuned to long wavelengths, M, tuned to medium wavelengths, and S, tuned to short wavelengths. In the retina, these photoreceptors are combined by specialised bipolar and ganglion cells which receive opponent input from the L and M cones to form the L-M pathway and opponent input of S and the sum of L and M outputs forms the S-(L + M) pathway (Dacey & Lee, 1994). The signals generated in them are relayed along the axons of the ganglion cells to separate layers in the lateral geniculate nucleus (LGN) which has a specific cytoarchitectonic structure. The L-M signal projects to parvocellular layers, while the S opponent signal projects to the koniocellular layers (for review see Martinovic, 2014). A third pathway projects to the magnocellular layers of the LGN and is commonly referred to as L + M + S, though debate remains about the inclusion of S cones (Chatterjee & Callaway, 2002; Sun et al., 2006). While parvocellular and koniocellular layers of the LGN include projections from ganglion cells that are colour opponent (Conway, 2009), it should be noted that not all cells in these layers are colour opponent (Sincich & Horton, 2005). This means that chromatic signals are not totally segregated from achromatic signals as early in the visual system as the thalamus.

From the LGN, the parvo, magno and konio pathways project to primary visual cortex. In the macaque monkey, magnocellular projections terminate in layer 4Cα, parvocellular projections terminate in layer 4Cβ, and koniocellular projections terminate in layer 2/3 blobs (sometimes called patches) (Sincich & Horton, 2005; Van Essen & Gallant, 1994). That each pathway terminates in separate layers of V1 lead early researchers to believe that signals from magno, parvo and konio cellular layers in LGN, remain segregated, and thus, independent, at this cortical level (Livingstone & Hubel, 1988). However, this picture is overly simplistic, as the signals intermingle extensively beyond their input layers. For example, many studies emphasise that magnocellular inputs in layer 4Cα project to layer 4B, but layer 4Cα actually projects more densely to both blobs and interblobs of layers 2/3 which are associated with parvo- and konio- cellular projections respectively,

* Corresponding author.
E-mail address: rebecca.lowndes@york.ac.uk (R. Lowndes).

https://doi.org/10.1016/j.visres.2024.108398
Received 12 December 2023; Received in revised form 24 March 2024; Accepted 24 March 2024
Available online 29 March 2024

implying early mixing of the chromatic (parvo and konio) and achromatic (magno) streams (Callaway & Wiser, 1996).

Most neurons in primate V1 which respond to chromatic stimuli also respond to achromatic stimuli (Johnson et al., 2008; Shapley & Hawken, 2011) meaning that their responses are driven by both chromatic and luminance signals. Solomon and Lennie (2005) found that colour-luminance cells in V1 show normalisation primarily driven by achromatic contrast inputs. This suggests therefore that chromatic responses are influenced by achromatic responses in visual cortex, but perhaps not vice versa. Contrast normalisation is consistently shown to be a property of single cells responding to combinations of signals in the cat primary visual cortex (Bonds, 1991; Heeger, 1992; Ohzawa et al., 1982; Ohzawa et al., 1985). Contrast normalisation, usually modelled as divisive, shifts response sensitivity of a neuron to account for ambient features in the image encoded by other neurons and while this normalisation has been most often shown in the visual domain, it is considered canonical to neural computation across domains as well as species (Carandini & Heeger, 2012). Contrast normalisation therefore offers candidate models to account for interdependence of chromatic and achromatic responses in visual cortex.

Psychophysical studies have long sought to capture the behaviour of chromatic mechanisms independent of achromatic mechanisms. This is normally achieved by presenting isoluminant stimuli to silence achromatic mechanisms. Isoluminance is a challenge to specify, particularly over large areas of the visual field because wavelength dependent pre-receptoral absorption due to macular pigmentation varies over the retina (Chen et al., 2001; Davies & Morland, 2004; Hammond et al., 1997; Ruddock, 1963; Snodderly et al., 1984), as does the morphology of cone outer segments (Goodchild et al., 1996; Smith & Pokorny, 1975; Srinivasan et al., 2008). This led Barbur and colleagues (1994) to present chromatic modulations superimposed on dynamically changing luminance checks to access mechanisms sensitive to chromatic modulations alone. The thresholds for detecting chromatic modulations were largely independent of the contrast of the background checks up to 35 % achromatic contrast, lending support to independence, particularly at threshold. However, there was a linear increase in the contrast detection threshold of achromatic gratings with increasing contrast of the random checked background. That is, the increase in contrast of the random luminance checked background made it progressively more difficult to detect achromatic target stimuli. This shows that the responses to the achromatic target grating and achromatic background are, predictably, interdependent, as a change in one component of the stimulus affects the detection of another, suggestive of a single mechanism processing both the background and target. This is consistent with earlier increment threshold work, which show that increment thresholds increase with overall luminance of the stimulus (Cornsweet & Teller, 1965).

Other psychophysical work has sought to understand how interactions, driven primarily by a presumed contrast normalisation mechanism, can be characterised. Due to the orientation tuning of neurons in V1, cross orientation gratings should be stimulating independent populations of neurons. Thus, dependence of the threshold for detecting target gratings on the contrast of a background grating at a different orientation could indicate contrast normalisation. Psychophysical work on cross-orientation gratings has shown that achromatic gratings of increasing contrast increase the detection threshold of achromatic target gratings and that this effect can be accounted for on the basis of divisive contrast normalisation (Baker et al., 2007; Meese & Holmes, 2010; Petrov et al., 2005). Similarly, the detection threshold of chromatic grating targets cross-oriented with chromatic grating backgrounds also increases with background contrast (Medina & Mullen, 2009). Important for the current study is the further work using spatially identical gratings as background and target that showed increasing contrast modulation along many chromatic directions, including achromatic, can increase the contrast detection threshold along many other chromatic directions (Chen et al., 2000a). This increase in contrast detection threshold points to interdependence of achromatic and chromatic mechanisms. The authors also demonstrated that such interdependencies could be captured by a divisive contrast normalisation mechanism (Chen et al., 2000b). For a review of chromatic and luminance noise masking research, see Eskew (2009).

Much like psychophysical approaches, neuroimaging research on human colour vision has largely sought to examine chromatic and achromatic response properties of the brain separately (for review see Wandell et al., 2006). Previous work has demonstrated that BOLD responses to S cone stimuli are significantly higher relative to their detection threshold compared to responses to L-M stimuli relative to their detection threshold (Lowndes et al., 2023; Mullen et al., 2007). Wade and colleagues (2008) used a random luminance background similar to Barbur (1994) and found that L-M responses were approximately double the responses to L + M + S contrast. A random luminance background method was also used in a recent study in our lab to show that detection thresholds for colour stimuli reflect neural signals found in visual areas V1, V2 and V4, in the case of the longstanding psychophysical effect of increasing spatial frequency decreasing sensitivity to chromatic stimuli (Lowndes et al., 2023).

Relatively fewer fMRI studies have combined achromatic and chromatic responses. Engel, Zhang and Wandell (1997) presented gratings with different degrees of chromatic and achromatic signal varying from chromatic modulations alone to achromatic alone. The results showed that in cone contrast space cortical responses were larger for chromatic than for achromatic modulations in both L against M and S against (L + M) chromatic planes. Similar to our previous work, they showed a tight coupling between behavioural contrast detection thresholds and V1 and V2 responses for most of the stimulus conditions. Another study investigated the V1 response to chromatic directions around the L and M contrast plane (Barnett et al., 2021) and found that V1 was most responsive to modulations in the L-M direction at 0 cycles per degree (CPD) and that the tuning largely followed a quadratic law indicating interactions of chromatic and achromatic signals.

The current study aimed to investigate the nature and extent of interdependence of cortical responses to chromatic and achromatic stimulus components. Our second aim was to investigate whether the way cortical responses combine can predict contrast detection threshold measurements. To achieve these aims we presented chromatic targets (L-M and S cone) at different contrasts superimposed on a background of checks that also varied in contrast, in fMRI. We found an interdependence of achromatic and chromatic cortical responses in V1 demonstrated by a reduction in chromatic responses at high achromatic background contrast. We also conducted a behavioural detection threshold study that showed a significant increase in contrast detection threshold of the chromatic targets with increasing achromatic background contrast, again indicating an interdependence of chromatic and achromatic mechanisms. Both the fMRI and behavioural data were best fitted by a model that included contrast normalisation of chromatic signals. Our examination of extrastriate regions revealed an increasingly compressive response to the achromatic background which was also smaller in magnitude at more anterior regions of the visual hierarchy. However, responses to the colour target did not become any more compressive and in many cases were of the same magnitude up the visual hierarchy. Maintaining a large dynamic range for encoding colour, while reducing it for achromatic variations may offer a useful representation of visual information for perception.

2. Methods

2.1. Participants

2.1.1. fMRI experiment

Seven (seven female) colour-normal trichromats (confirmed with Ishihara's tests for colour blindness, 38 plates edition) with a mean age of 27.17 years (+- 4.58 years) were recruited for four 60-minute experimental fMRI sessions, and one retinotopy session. The ethics

committee at York Neuroimaging centre at the University of York approved the experiment.

2.1.2. Behavioural experiment

12 (9 female) colour-normal trichromats (confirmed with Ishihara's tests for colour blindness, 38 plates edition) with a mean age of 29 years (+- 5.10 years) were recruited for three 50-minute behavioural sessions. The ethics committee at York Neuroimaging centre at the University of York approved the experiment.

2.2. Experiment and stimulus design

All visual stimuli were designed and presented using PsychoPy and PsychToolBox in MATLAB. The delivery system used for the visual stimulus in the scanner was a ViewPixx projector which projected the stimulus onto a custom-made acrylic screen. The participant viewed the screen with a mirror fixed to the head coil in the scanner. Behavioural stimuli were displayed using a ViewPixx monitor. Spectral measurements of the RGB channels of the scanner and behavioural screen were made using a 'Jaz' (Ocean Optics, FL) spectrometer. Chromatic stimuli were defined using the 10-deg cone fundamentals based on the Stiles and Burch 10-deg CMFs described in Stockman and Sharpe (2000). All stimuli were specified in terms of cone contrast. No further accounting for luminance for the individual participants in this study was conducted, so if presented on a uniform background the gratings we generated could contain luminance artefacts. However, the random luminance modulation described is an effective way of rendering many of these artefacts invisible and thus supress any neural responses to achromatic artefacts. There are also some benefits to showing physically identical stimuli to all participants, as this provides consistency across participants and sessions.

2.2.1. Retinotopy stimuli

Of the seven participants that completed the fMRI experiment, six took part in retinotopy scans as described. One participant had good retinotopy previously available from another visual neuroscience experiment (Vernon et al., 2016).

The retinotopy stimulus used was identical to that used in our previous paper (Lowndes et al., 2023) and similar to that described in other work (Alvarez et al., 2015; Binda et al., 2013; Dumoulin & Wandell, 2008; Welbourne et al., 2018). 1.25 degree wide sweeping bars moved in 8 bar directions across a 20 degree diameter circular aperture with four blank periods. The bar moved in steps once for every TR length (2500 ms) in 16 steps per direction, and contained 100 % contrast noise, updating at 2 Hz. Participants preformed a button press when the fixation cross changed as an attentional task to aid fixation. Four repeats were carried out for each participant.

2.2.2. Stimuli - fMRI experiment

The stimuli used for this experiment were adapted from Birch et al (1992) and similar to that used by another study from our lab (Lowndes et al., 2023). The 'background' stimulus consisted of an array of 100x100, 0.2 degree checks, which were each assigned a grayscale value that deviated a random amount from uniform grey between five different values for different trials: ±3.125, 6.25, 12.5, 25 or 50 % L + M + S contrast. The random contrast of each check was updated every 0.05 s (20 Hz). Superimposed target gratings were additional modulations that added either L-M (0 %, 0.3 %, 0.6 %, 1.3 %, 2.7 %) or S cone (0 %, 1.313 %, 2.625 %, 5.25 %, 10.5 %) contrast. This led to 25 compound stimuli for each colour condition which subtended the entire background (20 degrees). Orientation of the target grating was vertical and contrast polarity was reversed at a rate of 1 Hz in a square-wave function. A circular mask (diameter of 20 degrees) was applied to the stimuli. The spatial frequency of the grating was chosen to be 1.25 cpd and was presented in a square-wave pattern. This was the same as the lowest spatial frequency used in a previous study in our lab which used a similar background to investigate spatial frequency differences between S cone and L-M stimuli (Lowndes et al., 2023). In that previous study, we showed BOLD responses were very similar for both chromatic conditions at 1.25 cycles per degree and 2.7 % and 10.5 % contrast for L-M and S cone, respectively. Using the same spatial frequency here, as well as selecting previously used contrasts as our highest contrasts, gives us precedent to predict that responses to each colour direction will be similar. Additionally, the relatively low spatial frequency we have chosen allows us to discount the effects of chromatic aberration, as this has an influence at higher spatial frequencies (Bradley et al., 1992; Murasugi & Cavanagh, 1988).

To further ensure that chromatic aberration would not affect our findings, we used the equation detailed by Strasburger et al (2018) to calculate the diameter of blur given as:

$$b^{\circ} = 0.057PD$$

where P is the pupil diameter in millimetres and D is the defocus in dioptres. Eye recordings were taken of participants while they were taking part in the fMRI experiment. We found that pupil diameter was 3.19 mm on average. D has been calculated as ± 0.5 in previous work over the eccentricities used in this study and over similar wavelengths (458–632 nm) to the projector limits in our study (455–625 nm). We can therefore calculate the diameter of blur to be 0.091 degrees, which would extend 0.045 degrees on either side of grating boundary. With a grating bar width of 0.4 degrees, blur from extending from each boundary is not sufficient to cover the majority of the bar width (2 x 0.045 degrees), leaving 0.309 degrees of each bar unaffected by blur and thus at the specified contrast.

A rapid event-related design was used to present the 25 unique compound stimulus types in each condition (L-M or S), with each stimulus being displayed for 2 s, 10 times in a session. The trial order and the inter-trial intervals were optimised by using Optseq2 (Dale, 1999), which we applied to generate eight unique trial orders that each lasted 1940 s. Participants were randomly assigned one of the eight unique trial orders for each session. As this long run would be arduous for participants, it was split into five, 388 s runs, all to be completed in order in one scan session for each participant. Each trial run was padded with an extra 20 s of fMRI acquisitions at the end to ensure a return to baseline, so each run comprised 408 s. We conducted four sessions (in which 5 runs were presented) per participant; in two sessions we acquired responses to L-M target gratings and in the other two we acquired responses to S target gratings.

2.2.3. Stimuli – Behavioural experiment

Behavioural experiments were performed using a VIEWPIXX display using a two-interval forced choice paradigm. The background, present for the entirety of each run, comprised an array of 100x100 squares (0.2x0.2 degrees squared) with a 20 degree circular mask at five levels of achromatic contrast (3.125, 6.25, 12.5, 25 or 50 %) which changed between runs (see Fig. 1). Target stimuli were chromatic square-wave gratings which subtended the entire background at 1.25 cpd and were either L + M + S, S cone or L-M cone contrast. First, participants used a sliding scale to estimate their threshold (pressing up and down to increase and decrease contrast until they could just see the target grating), and this was used as the starting contrast for a staircase. Target stimuli occurred during one of two potential 0.5 s presentations, with each potential presentation indicated by the fixation changing from a standard fixation (+) to a cross (x). Potential presentations were separated by a 0.5 s interval. One presentation time contained a grating and one did not. If the target grating was present in the first presentation, participants were instructed to press '1′, if it was in the second presentation, they were instructed to press '2′. A standard three-up one-down staircase adjusted the contrast and the task finished after 16 reversals or 100 trials. The ~80 % threshold was calculated as the mean of the contrast during the last 7 reversals. If there were fewer than 7 reversals in a run,

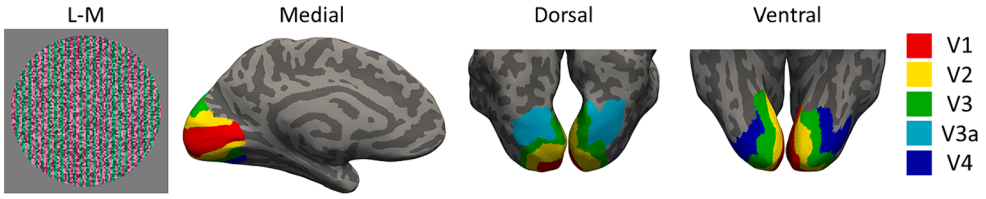

Fig. 1. Leftmost panel: an example of high contrast background stimuli with a high contrast L-M overlay. The L-M contrast has been artificially increased above the maximum used in the experiment for visibility. Right panels: The medial dorsal and ventral views of the ROIs used for one participant.

the participant was asked to return and complete this run again, beginning at a lower contrast.

2.3. MRI protocol

All scans were carried out using a Siemens 3 T MRI scanner, with a 64-channel head coil. The subject's head was positioned in the coil with foam padding to ensure the head was stable.

2.3.1. Retinotopy

76 EPI slices were taken within an FOV of 192x192mm with 1.5 mm isotropic voxels (TR = 2500 ms, TE = 40.8 ms, flip angle = 75°, voxel matrix = 128x128). Scan slices were aligned horizontally and always covered occipital and temporal lobes. Four retinotopy scans were taken for each participant.

2.3.2. fMRI experiments

36 EPI slices were taken within an FOV of 200x200mm with 2.5 mm isotropic voxels (TR = 1000 ms, TE = 30 ms, flip angle = 75°, voxel matrix = 128x128). Scan slices were aligned horizontally and always covered occipital and temporal lobes. A camera was positioned pointing at the participants left eye for blink monitoring and pupil diameter calculations.

2.3.3. Structural

In addition to functional scans, a T1-weighted and T2-weighted structural scan were taken for each subject, at a 0.8x0.8x0.8 mm resolution. The protocol for these scans was taken from the Human Connectome Project (Glasser et al., 2013).

2.4. Data processing

2.4.1. Structural

All structural scans were analysed using the HCP minimal processing pipeline (version 5.0, Glasser et al., 2013) using a combination of FSL (http://fsl.fmrib.ox.ac.uk/fsl/fslwiki/)(Smith et al., 2004) and Freesurfer (https://surfer.nmr.mgh.harvard.edu/) (Dale et al., 1999; Reuter et al., 2012).

2.4.2. Retinotopy

All data processing of retinotopy scans was performed using the 2015 version of the VISTA software (https://web.stanford.edu/group/vista/cgi-bin/wiki/index.php/Software) (Vista Lab, Stanford University), running under MATLAB 2015 (The MathWorks Inc., Natick, MA, USA). We applied pRF modelling to an average of all retinotopy scans (which had been motion corrected between and within scans using a maximum likelihood alignment routine (Nestares & Heeger, 2000)). Functional scans were aligned to individual anatomy scans using FLIRT linear registration (Jenkinson et al., 2002; Jenkinson & Smith, 2001). The retinotopic eccentricities and polar angles extracted by the pRF model were then used to draw boundaries of visual areas V1, V2, V3, V3a and V4 on a flattened representation of visual cortex; for details of the pRF model used and an example of drawn visual area boundaries, see Lowndes et al (2023). These regions of interest (ROIs) were then transformed into NIFTI files using the VISTA function roiSaveAsNifti and compared against an anatomically defined retinotopy atlas to ensure accuracy (Benson et al., 2014).

2.4.3. fMRI experiments

All five runs in a single session were concatenated to form a single run for analysis. All data were pre-processed using FSL version 5.0. Images were skull-stripped using a brain extraction tool (BET Smith, 2002). Motion correction (MCFLIRT; Jenkinson et al., 2002) was followed by spatial smoothing (Gaussian full width half medium 5 mm). Data were high pass temporal filtered (Gaussian-weighted least-squares straight line fitting with sigma = 50.0 s). Individual participant data was registered to their own high resolution structural (generated from T1 and T2 structural images using the HCP processing pipeline) using FLIRT (Jenkinson, 2001, 2002).

Previous work has shown that signals elicited by blinks may be a source of noise in fMRI signals (Gouws et al., 2014; Hupé et al., 2012), so we assessed the eye blinks in each scan to remove them as regressors of no interest. Each eye video was trimmed to the scan length and then split into individual frames. The structural similarity index measure (SSIM) (Wang et al., 2004) was calculated for consecutive image frames, low frequency movement (eg head movement) was excluded by subtracting a five-second windowed moving average from the measures, then instances of SSIM values in the lowest 5 percentiles were labelled as blinks. These were then manually confirmed. Eye blinks were then added as regressors of no interest into further analysis. One participant performed blinks infrequently (~3 blinks during a 7-minute scan), so the lowest 1 percentile was used for this participant, with blinks then manually confirmed again. The eye camera failed to record in 2 of the 42 sessions. Analysis was the same for these sessions but without this regressor of no interest.

Time-series statistical analysis was carried out using FMRIB's Improved Linear Model (FILM) with local autocorrelation correction (Woolrich et al., 2001). fMRI Expert Analysis Tool (FEAT)query was then run for visual areas V1, V2, V3, V3a and V4 with contrast of parameter estimate values converted into mean percentage signal change. For each participant, mean percentage signal change values were then averaged over the two sessions for each colour condition.

2.5. Model development

Our aim was to determine the extent to which responses to the chromatic target were dependent on the achromatic background, and potentially vice versa. We therefore fitted responses to the two components of the stimulus with one model that captured independence and two others that captured interdependence. We deployed the Naka-Rushton relationship in all models, which has been shown in numerous studies to model the achromatic contrast response function accurately in V1 of animals (Albrecht & Hamilton, 1982; DeAngelis et al., 1993) and humans (Rahimi-Nasrabadi et al., 2021). We note also that our form of the equation does not include exponent terms for the variables I and C, which are often introduced and can account for 'dipper functions' that emerge at low background contrasts. We have not removed the terms because we believe they are not useful in general, rather, our background and target contrasts are ones that are unlikely to reveal dipper-like behaviour and therefore we anticipated having little

or no data to inform on the exponent parameters. We adopt the 'exponent-free' form of the Naka-Rushton for all models. Reducing the number of free parameters in the model should also help distinguish between models. Interdependence was captured using divisive contrast normalisation, which has been shown widely in the literature to account for neural and behavioural responses (Chen et al., 2000a, 2000b; Heeger, 1992; Solomon & Lennie, 2005). Additionally, these models assume linear pre-cortical receptive fields, as has been shown to be consistent with previous data (Foley, 1994; Foley & Chen, 1997; Georgeson et al., 2016), although we note there can be early non-linearities.

Our first model assumes that the neurons responding to chromatic and achromatic components of the stimulus are independent, and thus the BOLD response should be as well. If the responses are independent, the responses to each component, chromatic and achromatic should sum linearly. Thus, our first model is a four-parameter model containing two Naka-Rushton equations summed together, henceforth referred to as the independent model:

$$R = RImax\,\frac{I}{I+I50} + RCmax\,\frac{C}{C+C50} \tag{1}$$

Where R is the BOLD response in percent signal change, I is the contrast of the achromatic component of the stimulus, RImax is the maximum response to I, and I50 is the contrast level of the achromatic background at which the achromatic response has reached half of RImax. C is the chromatic contrast, RCmax is the maximum response to C and C50 is the contrast level of C at which the response to colour has reached half of RCmax. This model cannot account for any changes in response to chromatic contrast that depend on achromatic contrast, or vice-versa, and thus, would predict no change in chromatic detection threshold with increasing background contrast in our detection threshold experiment.

A contrast normalisation model has been used before to account for detection thresholds for stimuli combining chromatic and achromatic components (Chen et al., 2000b). In line with this work, we first tested a simplified version of the model originally proposed by Chen and colleagues (2000b) by incorporating divisive normalisation for the response to chromatic contrast dependent on the achromatic contrast as follows:

$$R = RImax\,\frac{I}{I+I50} + RCmax\,\frac{C}{C+kI+C50} \tag{2}$$

Where k is a constant. This model will from now on be referred to as the selective chromatic contrast normalisation model. We also decided to mirror Chen et al.'s approach more closely by allowing achromatic contrast to affect the response to chromatic contrast (as above), and chromatic contrast to affect the response to achromatic contrast, as follows:

$$R = RImax\,\frac{I}{I+jC+I50} + RCmax\,\frac{C}{C+kI+C50} \tag{3}$$

Where j and k are constants. This model will be referred to as the mutual chromatic-achromatic contrast normalisation model. We have therefore defined three models with the first accounting for only independent responses to the two stimulus components and the remaining two accounting for interdependence of responses.

Our detection threshold data will be critical in determining whether the first model, with complete independence of chromatic and achromatic responses, is correct, as the model predicts no change in chromatic detection threshold with increasing background contrast. Models two and three would both allow for some change in chromatic detection threshold with increasing background contrast as has been previously reported by Chen et al., (2000a).

2.6. Assessing model validity

Model fits were calculated using the Matlab function *fminsearch* which allows the minimum values of a multiparameter function to be found. We reran fminsearch with adjusted starting parameters whenever a parameter would be above 1000. Akaike's information criterion (AIC; Akaike, 1974) was then used to evaluate the goodness of fit for each model, taking into account the benefit of any additional parameters. The AIC value for a model is defined as:

$$AIC = 2p - 2\log(L)$$

Where L is the likelihood of the residuals of the model fit and the data, and p is the number of model parameters. AIC values are arbitrary and thus can only be compared for models of the same dataset. The model that enumerates the lowest AIC score for one set of data has the best fit of the models tested. For the fMRI datasets, AIC values were calculated using the residuals of the data averaged across sessions and participants.

We then asked whether the model fits of the BOLD responses in V1 could predict the behavioural thresholds. Using the parameters for model fits found in the fMRI results, we first found the achromatic response alone, with chromatic contrast set to zero. This reduces all three models to the same equation but with different parameter values for RImax and I50 for each model and chromatic direction:

$$R_I = RImax\,\frac{I}{I+I50}$$

Where R_I is the response to achromatic increments only, calculated at each contrast level of I.

The fMRI model of the response (R_I) was then transformed using the following equation:

$$T_I = j\,\frac{1}{\frac{dR_I}{dI}}$$

where T_I is the model predicted detection threshold for achromatic target gratings at each background contrast level of I, j is a constant, and $\frac{dR_I}{dI}$ is the gradient of the modelled fMRI response to achromatic contrast (R_I) with respect to the achromatic contrast (I). Then a further fminsearch was performed in MATLAB with one free parameter (j) to fit on the log of the model predicted threshold and the log of the behaviourally measured thresholds. Note that this new parameter j only shifts the predictions of threshold up or down the vertical axis in figures and does not affect the shape of the predicted curves/lines.

Subsequently, we wanted to investigate whether the models could be used to predict the chromatic responses. Chromatic contrast can be modelled as the following in the independent model:

$$R_C = RCmax\,\frac{C}{C+C50}$$

In the models including chromatic response dependence on achromatic contrast, R_C can be modelled as:

$$R_c = RCmax\,\frac{C}{C+kI+C50}$$

Which is calculated at each level of I.

Again, using the parameters found using the fMRI data, R_C was then calculated for each model then transformed using the following equation:

$$T_C = j\,\frac{1}{\frac{dR_C}{dC}}$$

where T_C is the model predicted threshold and $\frac{dR_C}{dC}$ is the gradient of the modelled fMRI response to chromatic contrast (R_C) increments with respect to chromatic contrast (C) when C is very small, calculated at

each level of I. For the independent model, there is no dependence of chromatic response on achromatic contrast, so this model will predict no change in chromatic contrast detection threshold with increasing achromatic contrast.

AIC values were then calculated on the residuals of the log behavioural threshold data, and the log of the model predicted thresholds. Log values were used to ensure that the higher contrast background (50 %) results were not unduly skewing the results, as this was sometimes an order of magnitude higher than the threshold values with the lowest background contrast, particularly in the achromatic condition.

3. Results

Firstly, we assessed the *reliability of fMRI results (3.1)* we acquired across sessions and conditions, in order to determine whether our responses are consistent. Having ensured internal validity of our fMRI results, we will then be able to average and compare across different sessions and conditions. Secondly, the three models we have proposed will be fitted to our *V1 results (3.2)* to assess the extent of interdependence of responses to achromatic and chromatic stimulus components. We have chosen V1 as the primary area to investigate as it has direct connections to the pathways from the LGN, and may therefore maintain independence, or alternatively exhibit interdependence. Thirdly, statistics will be reported for the *detection thresholds (3.3)* to determine whether there is evidence of interdependence of chromatic and achromatic thresholds. Fourthly, we predicted detection thresholds from V1 responses *(3.4)* using the parameters we derived from V1 (3.2). This will allow us to assess which of the three models best account for behavioural thresholds as well as neural signals. Finally, we will then look at the responses to our stimuli in *extrastriate visual areas (3.5)* to see how signals are processed in more anterior regions.

3.1. Reliability of fMRI results

The first step in analysing the fMRI data is to assess the reliability of our data across sessions, as our intention is to average each participants' results across sessions for each condition. To ensure this is statistically appropriate, we have first correlated the percent signal change values calculated for identical conditions across sessions, the results of which are shown in the first two graphs in Fig. 2. There is a high correlation between results across different scan sessions which were performed on different days. This gives us confidence in averaging the results across sessions for the same condition. Secondly, the L-M and S condition sessions each contain five stimuli that are identical to each other, where achromatic contrast is present at five levels (3.125 %, 6.25 %, 12.5 %, 25 % and 50 %) but chromatic contrast is at zero. The rightmost graph of Fig. 2 shows the correlation between responses to these stimuli during L-M and S sessions. There is also a high correlation found here, showing good internal validity of our results. We also computed an adjusted R^2 value ($N = 25$) for each of the seven participants and for the L-M condition it varied between 0.48 and 0.85 with a mean of 0.67. For the S cone condition adjusted R^2 ($N = 25$) varied between 0.51 and 0.77 with a mean of 0.61. For the achromatic conditions adjusted R^2 ($N = 5$) varied between 0.70 and 0.98 with a mean of 0.86. This gives us confidence that we can further analyse our results, comparing across days and sessions knowing that responses to our stimuli are reproducible.

3.2. V1 Results

The aim of this section is to assess the fit of the three models to V1 responses to our stimuli. V1 has been selected as the first area to be examined since it is the first cortical area that processes visual signals, as well as the largest retinotopic representation of visual space (Dougherty et al., 2003). Also, we know that the LGN passes signals directly to separate layers of V1 for each visual pathway (Derrington et al., 1984) so if any cortical area would show independence of achromatic and chromatic signals, it should be primary visual cortex. Additionally, previous work has shown a coupling between fMRI responses in primary visual cortex and behavioural contrast detection thresholds (Engel et al., 1997; Lowndes et al., 2023).

Fig. 3 shows the result of our analysis of the 25 chromatic and achromatic combinations for both L-M (Fig. 3A) and S (Fig. 3B) responses, averaged across sessions, and across participants. In the upper and lower rows of panels a and b the same data are plotted as a function of the achromatic contrast (grouped by chromatic contrast) and chromatic contrast (grouped by achromatic contrast), respectively. Each column shows the same data repeated, with the lines in the first three columns representing the fits of the different models; independent, selective chromatic contrast normalisation (Selective Normalisation), and mutual chromatic-achromatic contrast normalisation (Mutual Normalisation). Looking solely at the fMRI data (represented by dots), there are robust increases in response in both achromatic (top rows Fig. 3a and b) and chromatic (bottom rows Fig. 3A and B) stimulus directions, with a larger increase in the achromatic direction. In both L-M and S cone conditions, there appears to be a greater dynamic range of chromatic response at low achromatic background levels. This is evidenced by what we refer to

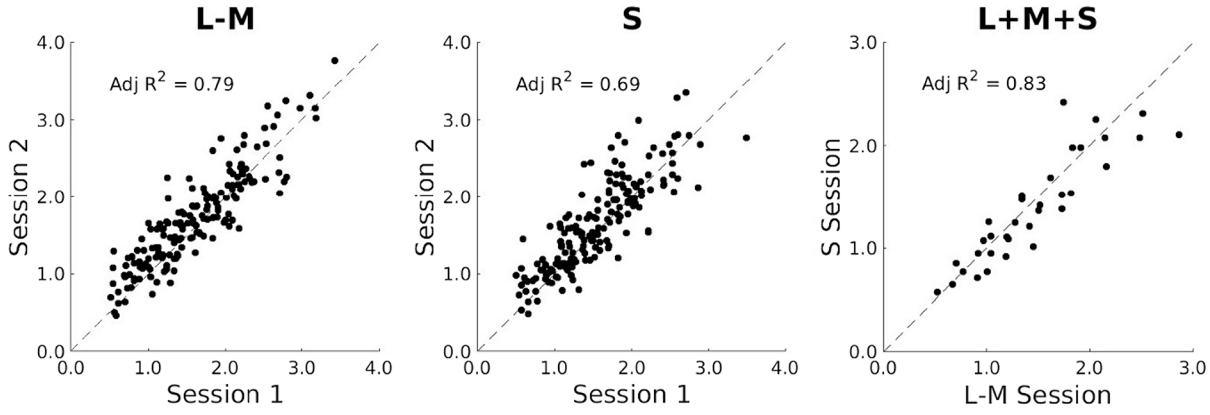

Fig. 2. A scatter graph (left) in which each data point is a percent signal change value in V1 for each stimulus level and participant in L-M session one, plotted against the percent signal change value for that same stimulus level and participant in L-M session two. The dotted diagonal line shows perfect correlation and the value in the top left is adjusted R^2. The middle graph shows a scatter graph plotted as before showing the correlation of each data point for S cone session 1 and S cone session 2. In the rightmost scatter graph each dot is a percent signal change value for each of the achromatic background contrast levels when the chromatic contrast level was zero, averaged across session one and session two for the L-M and S sessions. Since chromatic contrast is zero for these conditions, the stimulus is identical between the L-M and S cone scans, and therefore this plot shows achromatic responses with the same stimulus profile during different scans. Again, adjusted R^2 is shown in the top left. While the data are given here for all participants we also computed correlations for each participant separately (see text for details).

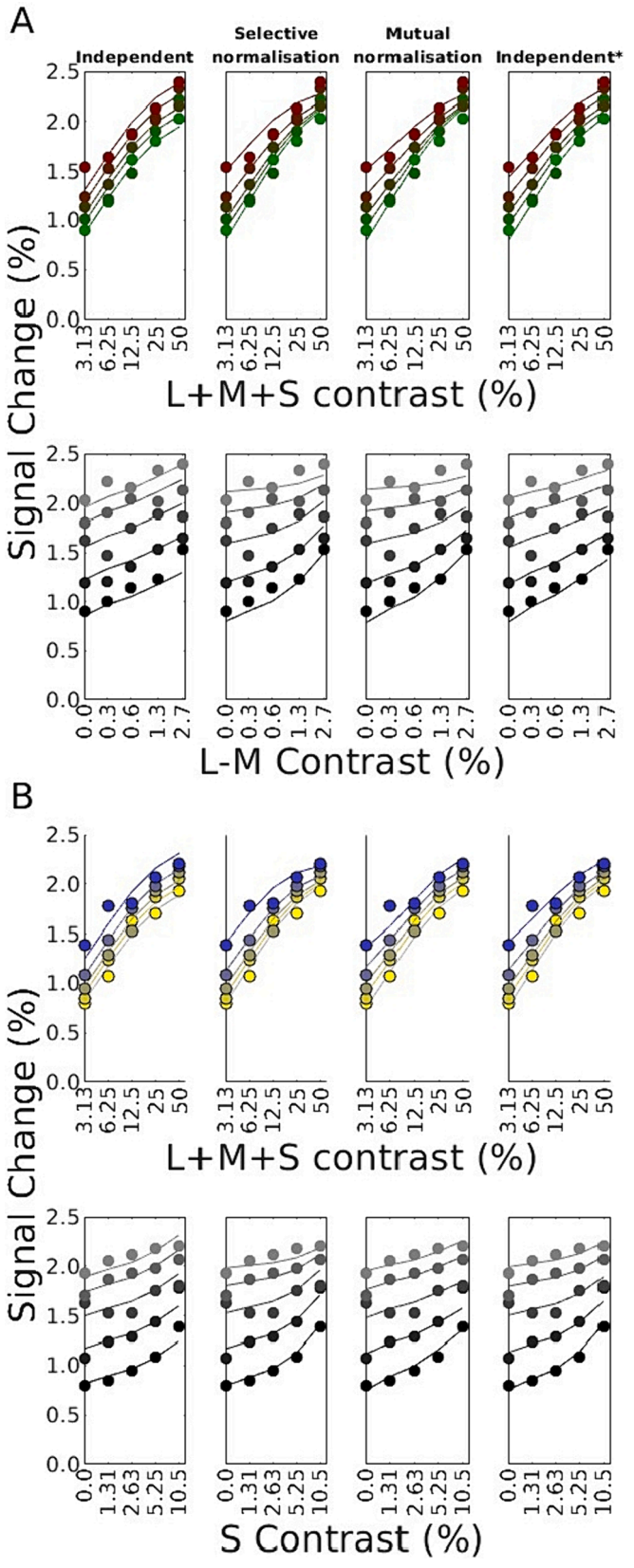

(caption on next column)

Fig. 3. A figure showing the percentage signal change averaged across all participants and both runs for all 25 stimulus conditions in the fMRI sessions. 3A, top panels are responses to L-M plotted along the achromatic contrast axis, with the chromatic contrast increasing from green to red. NB, the colour of these points is arbitrary, for example, the green coloured dot represents the response when the L-M contrast was zero. Fig. 3A, bottom graphs show the same data, this time plotted against the L-M contrast axis with the achromatic contrast increasing as the dots move from black to grey. The graphs in the first column show the independent model fits, the second show the selective chromatic contrast normalisation model fits, the third show the mutual chromatic-achromatic contrast normalisation model fits, and the fourth show the independent neural response with nonlinear BOLD model fits. (For interpretation of the references to colour in this figure legend, the reader is referred to the web version of this article.)

as a 'pinching' of the range of chromatic responses at higher achromatic background contrasts in the top rows of Fig. 3A and B. The corollary of the pinching in the upper data plots is the reduced gradient of chromatic responses as background achromatic contrast is increased in the bottom rows of Fig. 3A and B. These features of the data indicate some interdependence of chromatic and achromatic responses.

Fig. 3B shows the data from the S cone condition sessions in the same way, with the top row showing the achromatic contrast increasing along the x-axis and chromatic contrast going up from yellow to blue. The fourth shows S contrast increasing along the x axis with achromatic contrast going up from black to grey.

The lines in Fig. 3 represent the fit for each model tested. The first model, which assumes the responses to achromatic and chromatic stimulation should be completely independent, accounts for much of the variance quite well in the L-M and S cone condition (Fig. 3A and B, first column), but cannot account for the larger dynamic range of responses to chromatic contrast targets on a low achromatic contrast background compared to the dynamic range on higher achromatic contrast backgrounds. This is most obvious in the L-M condition where achromatic contrast is very low (3.125 %) and L-M contrast is high (2.7 %) which yields a higher response than the model would predict. By definition this model generates lines that are parallel in the plots and therefore cannot account for the observed pinching in the data plots of Fig. 3.

The two models incorporating interdependence using divisive contrast normalisation can account for pinching in the upper plots and correlated reduction in the gradient of the plots in the lower panels. There is a suggestion in the L-M condition that the dynamic range of the chromatic responses may have been compressed too much by the models at high achromatic contrast, which is especially evident in the mutual chromatic-achromatic contrast normalisation model.

AIC values were calculated for each model for L-M and S cone conditions separately, then summed together to show the model performance across conditions. The selective chromatic contrast normalisation model had a lower AIC value (-98.42) compared to the independent (-88.52) model and marginally lower than the mutual chromatic-achromatic contrast normalisation (-98.08) model. This indicates that of these three models, the selective chromatic contrast normalisation model is the most likely to explain our data.

In order to investigate the strength of the normalisation effect, we computed the modelled chromatic responses at each achromatic level, using the selective chromatic contrast normalisation model as an example (Fig. 4). The effect of the modelled normalisation is relatively strong, decreasing L-M responses by a factor of 4.16 and S responses by a factor of 3.03 between 3.13 and 50 % achromatic contrast. When using the mutual chromatic-achromatic contrast normalisation model, the L-M responses were reduced by a factor of 3.67 and S response by a factor of 1.66. It should be noted, however, that these are modelled responses, and the overestimate of pinching shown in Fig. 3 will have translated to these calculations and show a greater change due to contrast normalisation than may be present in the brain data, particularly in the L-M condition, where this effect is stronger.

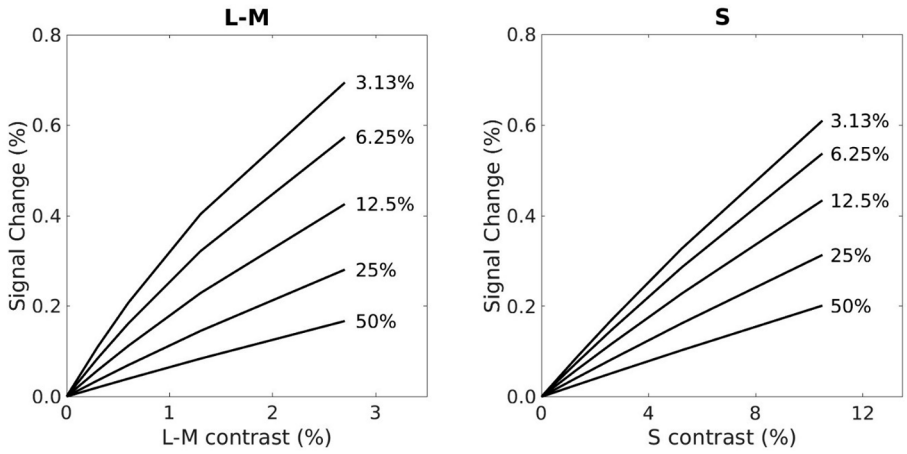

Fig. 4. A graph showing the modelled chromatic response to L-M (left) and S (right) contrast at each achromatic contrast level tested. Each individual line is a mean of the model fit of the chromatic response at the marked achromatic contrast level.

An alternative explanation for our fMRI results in V1 could be that achromatic and chromatic responses are combined independently as in our first model, but that there is some response nonlinearity between the neural response and our measured BOLD response. A nonlinearity is possible, but we note also that there is evidence that it is largely linear in V1 (Boynton et al., 1996). For completeness, however, we have added a fourth model, which assumes linear summation of the achromatic and chromatic responses is representative of the neural response (as shown in our first independent model) and this is followed by a compressive non-linearity of the sum of the neural response (again utilising the Naka-Rushton equation), which is shown in the furthest right column of Fig. 3. As shown, an assumption of non-linearity after combination of achromatic and chromatic neural signals fits the fMRI data in V1 well, in fact the AIC value was significantly lower for this model than any other tested (-113.44) suggesting this model is more likely to explain our data. However, as with the independent model, any model that has no dependence of achromatic contrast on chromatic responses will be unable to account for any changes in behavioural thresholds with increasing achromatic background contrast. As will be shown in section 3.3 and 3.4, we have found significant increases in detection thresholds with increased achromatic contrast, which are well predicted by our contrast normalisation models. Therefore, while investigating non-linearities of the BOLD response is an important avenue for further research, we will focus on the first three models that assume a linear relationship between the neural and BOLD response for the rest of this paper.

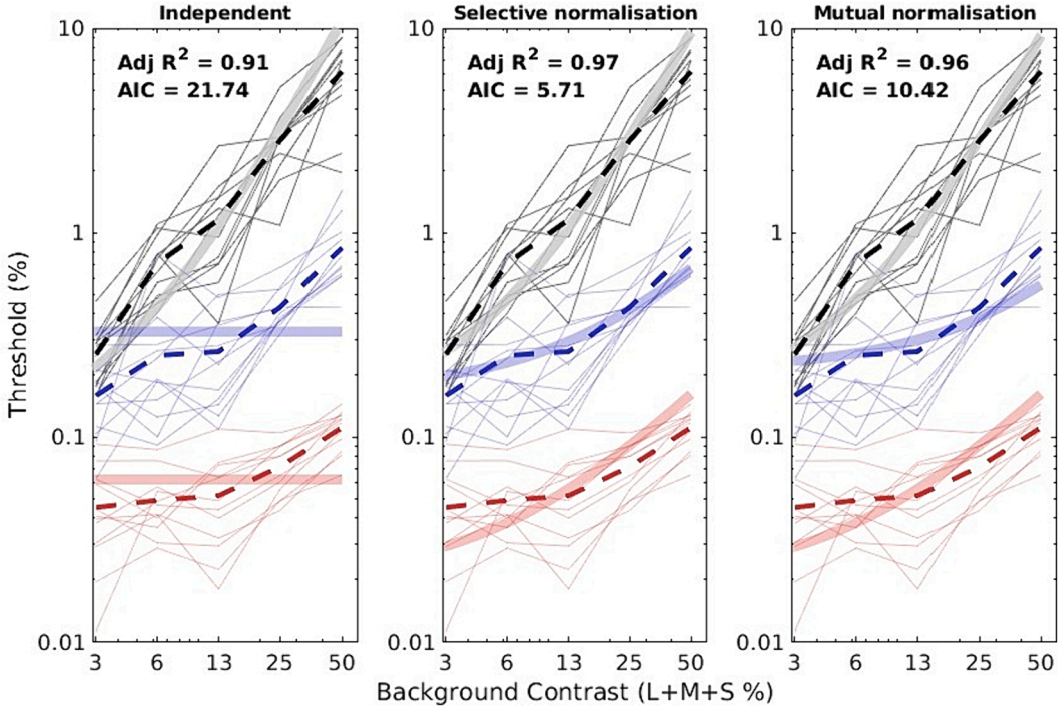

Fig. 5. A figure showing the behavioural thresholds obtained by individuals (thin light grey, blue and red lines) and the mean (dashed lines) for L + M + S, L-M and S colour directions against the different achromatic background contrast levels (3.125–50 %). Each graph displays the same data. The thick transparent lines show the model fit for each model as predicted in *V1 results (3.2)* for the independent, selective chromatic contrast normalisation, and mutual chromatic-achromatic contrast normalisation models. The AIC value at the top of each graph is the sum of the individual AIC values for each colour direction. (For interpretation of the references to colour in this figure legend, the reader is referred to the web version of this article.)

3.3. Detection thresholds

Given the outcome of the modelling above, we anticipate that contrast detection thresholds should vary with background contrast. The contrast detection thresholds are shown in Fig. 5, with three panels showing identical data but different model fits which we will explain in section 3.4. They reveal that the highest thresholds are found for achromatic stimuli, particularly at high achromatic background contrasts. Of the two chromatic directions, S cone detection thresholds were higher than L-M thresholds. The graphs show increases in all behavioural thresholds with increasing background contrast, although, as anticipated, chromatic thresholds increase far less than achromatic thresholds.

We examined whether thresholds changed significantly as a function of background contrast with a 5 by 3 (background contrast level by target colour condition) ANOVA. Greenhouse-Geisser correction to degrees of freedom was applied where sphericity violated. The analysis revealed significant main effects of background contrast ($F(2.62, 28.80) = 125.63$, $p = 4.43x10^{-16}$, $\eta^2 = 0.92$), and colour condition ($F(2, 22) = 611.39$, $p = 5.25x10^{-20}$, $\eta^2 = 0.98$) as well as a significant interaction ($F(8, 88) = 21.34$, $p = 1.20x10^{-17}$, $\eta^2 = 0.66$). This led us to perform subsequent one-way ANOVAs for each colour condition. In the achromatic condition, there was a significant effect of background contrast level ($F(4, 44) = 133.62$, $p = 5.18x10^{-24}$, $\eta^2 = 0.92$). There was also a significant effect of background contrast level in the L-M ($F(2.12, 23.33) = 21.30$, $p = .000004$, $\eta^2 = 0.66$) and S cone ($F(4, 44) = 36.04$, $p = 2.33x10^{-13}$, $\eta^2 = 0.77$). Post-hoc tests revealed that, in both chromatic conditions, this was driven by the two highest levels of achromatic background contrast (25 % and 50 %), as these thresholds were significantly higher than those at the lower background contrasts, and each other. In the achromatic condition, all five levels are significantly different from each other, indicating that the threshold increases significantly with each increase of the background contrast, with the exception of two middling levels of background contrast (6.125 and 12.5 %) not being significantly different from each other ($p = .195$). That there are significant increases in detection thresholds with increasing background contrast in both of the colour directions tested, confirms that there must be some interdependence of the signals from achromatic and chromatic pathways elicited by these stimuli.

3.4. Predicting thresholds from V1 responses

The model parameters found in section 3.2 (*V1 results)* were then used to predict thresholds as described in section 2.6 (*assessing model validity)* and are shown in the transparent coloured lines on Fig. 5. All three models predict the achromatic threshold data well. The independent model, shown in the left panel, cannot account for the changes in chromatic contrast detection threshold. This can be seen in Fig. 5 as flat responses to increasing achromatic background contrast. The selective chromatic contrast normalisation model, shown in the middle panel, predicts achromatic and S cone thresholds very well. The L-M model predictions generate a steeper curve than the detection thresholds we measured. Similarly, the mutual chromatic-achromatic contrast normalisation model, shown in the right panel of Fig. 5, predicts a steeper curve than we find for L-M thresholds, and to a greater extent than for the selective chromatic contrast normalisation model. The mutual chromatic achromatic contrast normalization model also predicts a shallower curve for the S cone thresholds than our detection threshold results show. On inspection of Fig. 5 therefore the detection threshold data appear best fit by the selective chromatic contrast normalisation model (middle column). This is also supported by the AIC values shown the panels of Fig. 5.

3.5. Extrastriate visual areas

In Fig. 6, we plot the contrast response functions for extrastriate visual areas V2, V3, V3A and V4 alongside those for V1. Fig. 6A shows the responses during the L-M condition, and Fig. 6B shows the responses during S cone conditions. The top row of A and B shows responses to achromatic contrast grouped by the chromatic target contrast and the

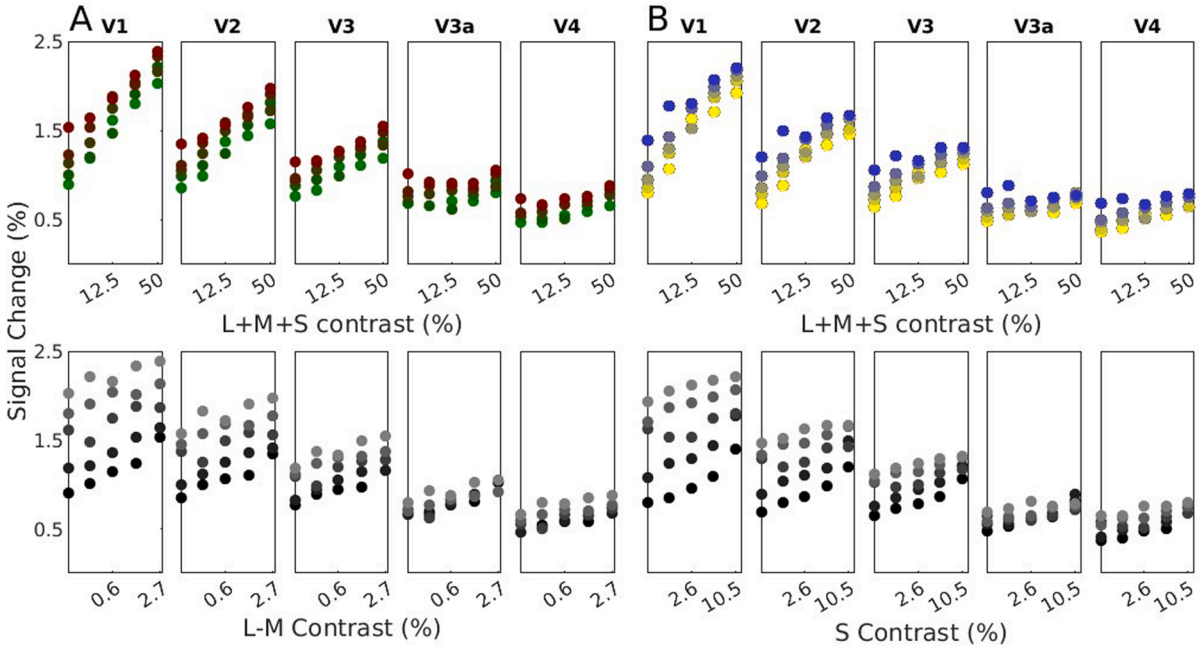

Fig. 6. A) Plots showing the average response to each stimulus in the L-M condition against achromatic contrast (upper) and against L-M contrast (lower) as described in Fig. 3, for each visual area (V1, V2, V3, V3a and V4). In the top panels, L-M contrast increases from green to red. NB, the colour of these points is arbitrary, for example, the green coloured dot represents the response when the L-M contrast was zero. In the bottom graphs, plotted along the L-M contrast axis, achromatic contrast increases as the dots move from black to grey. B) Plots showing the average response to each stimulus in the S cone condition against achromatic contrast (upper) and against S contrast (lower) as in A, with chromatic contrast increasing from yellow to blue. (For interpretation of the references to colour in this figure legend, the reader is referred to the web version of this article.)

bottom row shows responses to chromatic contrast grouped by achromatic background contrast. Inspection of the top rows show that higher up the visual hierarchy the range of response to achromatic contrast falls. This is largely due to the compression of responses to higher background contrasts. The corollary of this in the bottom row plots is the reduction in the vertical spread of the data up the visual hierarchy. The range of response to the target chromatic contrast appears better preserved across visual areas as shown by small changes in the slope of the responses in the lower panels and the relatively well-preserved vertical range of the responses shown by the coloured symbols in the upper panels.

We then plot the mean responses to achromatic contrast across chromatic contrast levels (top row) and the mean responses to chromatic contrast across achromatic contrast levels (bottom row) in each visual area for L-M and S cone conditions in the left column of Figure 7A and B respectively. There is a reduction in the achromatic responses in more anterior regions, coupled with an increasingly compressive response. Conversely, while there is a reduction in responses to chromatic contrast with anterior regions in the bottom plots of Figure 7A and B, the responses measured from each area remain reasonably parallel, maintaining their dynamic range. It must be noted however that all achromatic interactions with the chromatic responses are averaged in these plots.

To minimise the influence of achromatic contrast on the chromatic responses and vice versa we therefore plot achromatic responses in the absence of chromatic targets (top row) and response to the chromatic target in the presence of the lowest contrast achromatic background (bottom row) in the right hand columns of Figure 7A and B. The right column plots are largely similar for the achromatic responses in terms of their shape with compressive characteristics. For the chromatic responses however the gradient of the largely linear responses increases across all areas and appears more parallel, a feature that indicates that the background contrast interacts with the response to the chromatic target contrast in extrastriate cortex as well as V1.

We calculated and plotted (Fig. 7C) the difference between the responses to the highest and lowest achromatic contrasts (in the absence of a chromatic target), alongside the difference to the highest and lowest chromatic contrasts, for L-M (left) and S (right) conditions (for the lowest achromatic background contrast) to provide an empirically derived amplitude of the response range for each visual area to the contrast along different colour directions. The plots show the reduction in responses to achromatic contrast in more anterior visual regions, while the dynamic range of the chromatic responses is better preserved up the visual hierarchy. To assess this statistically, we performed a separate two-way ANOVA for each chromatic condition (visual area by colour direction). In the L-M condition, there was a significant interaction between visual area and colour direction ($F(4,24) = 23.96$, $p = 4.41\text{x}10^{-8}$, $\eta^2 = 0.80$). The interaction was also significant in the S condition ($F(1.93,11.60) = 21.03$, $p = .00065$, $\eta^2 = 0.78$). This led us to preform subsequent one-way ANOVAs for each condition, on achromatic and chromatic results separately. For the achromatic responses, there was a significant effect of visual area during both the LM ($F(4,24) = 21.08$, $p = 1.45\text{x}10^{-7}$, $\eta^2 = 0.78$) and S ($F(4,24) = 47.17$, $p = 4.97\text{x}10^{-11}$, $\eta^2 = 0.89$) conditions with high effect sizes. The effect of visual area was also significant for chromatic responses in both L-M ($F(1.99,11.94) = 8.93$, $p = .004$, $\eta^2 = 0.60$) and S ($F(4,24) = 6.97$, $p = .001$, $\eta^2 = 0.54$) conditions, but with lower effects sizes than were shown for achromatic responses. This shows that while chromatic responses do reduce up the visual hierarchy, this reduction is more dramatic for achromatic responses.

While it may be tempting to model the responses of extrastriate areas and then use those models to fit the behavioural thresholds, there is an issue with this approach. The steeper gradients observed for the achromatic responses in V1 compared to all other areas lead to greater sensitivity and therefore lower thresholds. While the chromatic responses appear more robust over visual areas, it is also true that the

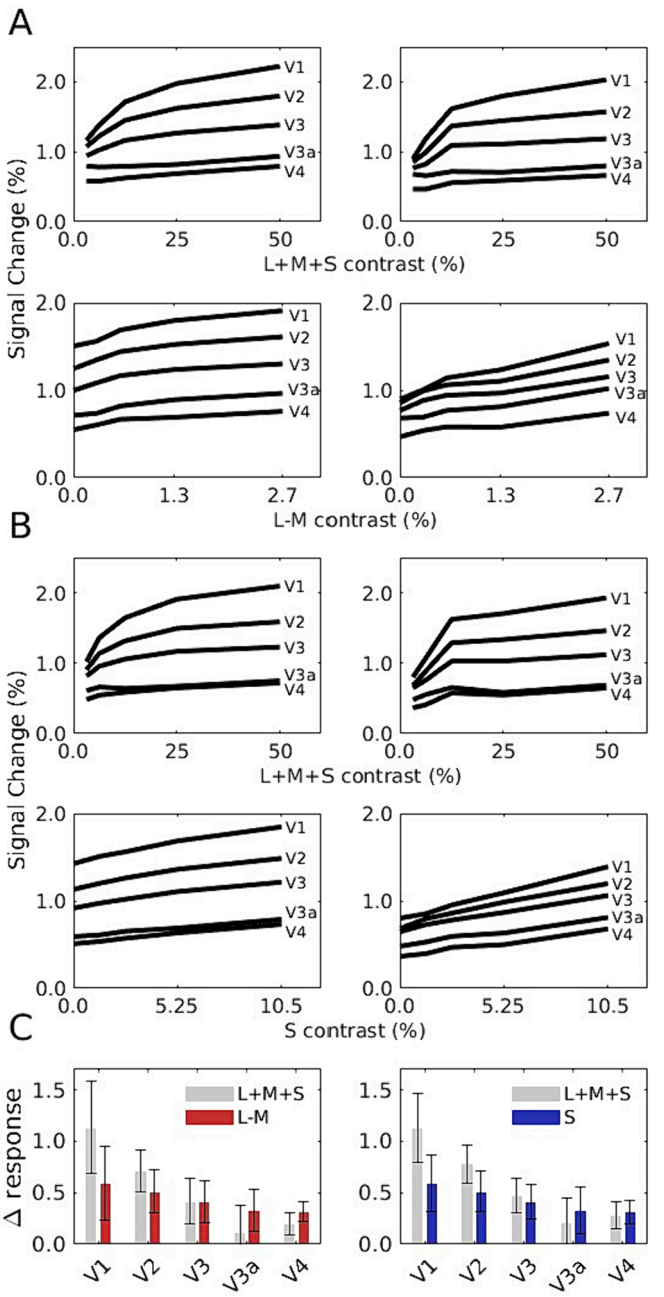

Fig. 7. A) Left column plots show the responses to achromatic contrast averaged across all L-M contrast levels (upper) and the responses to L-M contrast averaged across all achromatic contrast levels (lower) in each visual area. Right column plots show the response to 0% L-M stimulus contrast for each achromatic contrast level for each visual area (upper) and the response to the lowest achromatic contrast at each L-M contrast level (lower). B) As in A, left plots show the mean responses and right plots show the responses to the lowest level contrasts, now for the S cone condition. C) The left graph shows a bar chart displaying the difference (Δ) between the mean response to the maximum (50%) and minimum (3.125%) achromatic contrast for each visual area when L-M contrast is 0% in grey bars. The red bars show the difference in the response to the maximum L-M contrast (2.7%) and the minimum (0%) where achromatic contrast is at its lowest (3.125%). The right graph shows the difference (Δ) between the mean response to the maximum achromatic contrast (50%) and the minimum (3.125%) for each visual area when S contrast is 0% in grey bars. Blue bars show the difference between the maximum S contrast (10.5%) and the minimum (0%) where achromatic response is at its lowest (3.125%). Error bars are 1 standard deviation.

gradient of those responses reduces up the visual hierarchy, so again our model for thresholds would predict lower thresholds from V1 responses compared to those derived from any other visual area. Moreover, given the compressive nature of the achromatic contrast response function, the variance of the data is reduced considerably compared to the measurement error and therefore insights concerning the interdependence of signals and their relationships with thresholds are much more limited for responses from extrastriate areas.

4. Discussion

The aim of this study was to investigate the nature and extent of interdependence of brain responses to chromatic targets on achromatic backgrounds, and how they can explain target detection thresholds. From our fMRI experiment, we found that a model incorporating divisive contrast normalisation of chromatic contrast responses by achromatic contrast best explained our data in V1 out of the three models tested, closely followed by mutual normalisation of achromatic and chromatic responses by chromatic and achromatic contrast. The selective chromatic contrast normalisation model predicted detection thresholds best out of the models tested. We also found that achromatic responses reduced further up the visual hierarchy, while chromatic responses remained more consistent.

In our detection thresholds experiment, we found a clear increase in achromatic contrast detection thresholds with increasing achromatic background contrast. This is in line with the study by Barbur (1994) and suggests that despite differing spatial and temporal frequencies, these two stimulus components are generating responses in similar sets of neurons. Our study found more subtle increases in contrast detection threshold in both chromatic directions that only became significant at high (>= 25 %) background contrast. Barbur et al (1994) reported little change in chromatic contrast detection thresholds as achromatic background contrast increased, but examination of their plots does indicate that thresholds for gratings presented on 35 % compared to 8 % backgrounds were higher, which is consistent with our findings. Chen and colleagues (2000a) investigated the potential for interdependence of chromatic and achromatic thresholds using background masks and pedestal targets of different chromatic directions, but identical spatial and temporal properties. They found an increase in contrast detection thresholds of isoluminant targets corresponding to L-M (red-green) and S cone (blue-yellow) when achromatic backgrounds rose above 10 % contrast. This suggests, along with our work, that achromatic and chromatic responses are interdependent. Chen and colleagues (2000b) used divisive contrast normalisation to explain their findings.

Other psychophysics research has shown chromatic responses consistent with divisive contrast normalisation. Medina and Mullen (2009) showed that cross orientation masking effects are significantly greater for chromatic test stimuli on chromatic masks than for their achromatic counterparts. However, another study found that the cross-orientation masking effect did not occur with achromatic masks and chromatic test stimuli (Mullen et al., 2014). Given that we and Chen et al have found evidence for interdependence for stimuli that are not cross orientated, the normalisation of chromatic by achromatic signals may be specific to the relative orientation of the components.

Single-cell recordings of neurons in the primary visual cortex of macaques showed that V1 combines magnocellular and parvocellular inputs (Li et al., 2015), suggesting interdependence of the responses of these pathways. All chromatic cortical neurons show evidence of divisive contrast normalisation in macaque V1 (Solomon & Lennie, 2005) with the divisive pool being derived from a population representing more diverse response patterns. In humans, there is evidence in electrophysiology for non-linear summing of responses to the combination of chromatic and achromatic stimuli whereby the response to combinations were smaller than predicted by the sum of responses to the parts (Martinovic & Andersen, 2018). Taken together, this research shows that achromatic and chromatic signals are interdependently processed and that this can be shown in physiology. Our measurements of V1 responses are consistent with the physiological studies above and based on previous modelling approaches we explored further the nature of the interdependence of responses to chromatic and achromatic stimuli.

To uncover the source of the interdependence of chromatic and achromatic responses in early visual cortex, we deployed a simplified version of the contrast normalisation model outlined by Chen et al., (2000b) which accounted for mutually inhibitory combinations of chromatic and achromatic responses. Our modelling indicated that inhibition may be unidirectional, as the model that included only the chromatic response dependence on achromatic contrast, but not the achromatic response dependence on chromatic contrast, was found to be the most likely to explain our fMRI results in V1. It is possible that the achromatic stimuli we presented were highly potent, given their spatiotemporal characteristics and high contrast levels, and thus it may have a dominant effect on the normalisation pool, leading to any normalisation from the chromatic targets on achromatic responses to be undetectable. However, single unit recordings of neurons in V1 and V2 of macaques, have shown that among neurons that are responsive to both chromatic and achromatic stimuli, the normalisation pool is primarily driven by colour directions close to achromatic (Solomon & Lennie, 2005). Taken together with our work, there is evidence therefore that the pools used in divisive contrast normalisation can be selective.

We showed that a model of fMRI signals in V1 can predict contrast detection thresholds. The modelled changes in responses to chromatic target gratings with increasing achromatic background contrast predicted the increase in detection threshold of the same gratings with increasing background contrast, although the predictions were better for the S cone than the L-M direction. The modelled response to the background component of the stimulus alone was also able to predict the increases in detection thresholds for achromatic target gratings as background contrast increased, showing that there is a common mechanism for processing the target and background, when they are both achromatic even when they have different spatiotemporal properties. This offers reassurance that luminance artefacts of the chromatic gratings are unlikely to be registered in the brain responses we measured. Other work has also shown correlations between brain response and detection thresholds; contrast detection thresholds at many points of the L-M and S-(L + M) chromatic plane show a coupling with responses in V1 and V2, at temporal frequencies of 4 Hz and below (Engel et al., 1997). Previous work in our lab has shown that V1 responses relate well to the elevation of contrast detection thresholds when the spatial frequency of chromatic stimuli is increased (Lowndes et al., 2023).

We assumed that the relationship between the neural responses and the BOLD response is linear in our modelling framework. However, it is of interest that V1 responses can be modelled well with no interaction between neural responses followed by a compressive non-linearity, which could reflect a compressive non-linear relationship between the neural responses and BOLD. In the domain of vision there is evidence to support that the neural-BOLD response is linear (Boynton et al., 1996) and it is also true that when we introduced the non-linearity, the model would be incapable of predicting chromatic threshold elevations as a function of the achromatic background. So while it is of future interest to understand the relationship between BOLD and the neural responses that drive it (Logothetis et al., 2001), increasing the degrees of freedom to model it here is beyond the scope of our study.

In extrastriate visual areas (V2-V4) we found a smaller and more compressive response to achromatic contrast up the visual hierarchy, consistent with previous literature (Buracas & Boynton, 2007; Gouws et al., 2014; Liu & Wandell, 2005; Tregillus et al., 2021). The compression of responses further up the visual stream is more subtle in our chromatic response data. The results that chromatic information is better preserved relative to achromatic background information likely reflects the value of colour in identification or recognition of visual features that are processed higher up the visual hierarchy. We also found BOLD responses to S cone stimuli were remarkably similar to those

elicited by L-M stimuli. The cone contrasts of the stimuli eliciting these responses were however many more multiples of the psychophysically determined threshold for L-M than for S cone stimuli. S cone contrast has been shown to correlate better with BOLD response than a threshold based metric (Mullen et al., 2007). Similarly, our recent study found similar BOLD responses to S cone stimuli at 6.17 times threshold as L-M stimuli at 20.95 times threshold (Lowndes et al., 2023).

5. Conclusions

This study has provided new insight into the combinations of chromatic and achromatic responses in primary visual cortex of humans, and how they relate to behavioural responses. V1 responses were best predicted by a selective chromatic contrast normalisation model of the three models tested, showing that achromatic and chromatic responses are interdependent. Behavioural responses also showed dependence of the detection threshold for chromatic targets on achromatic background contrast, which was well predicted by the same selective chromatic contrast normalisation model. This study has shown that V1 responses align well with behaviour, suggesting that perception of these stimuli is set at this early cortical stage. A large dynamic range was maintained for encoding colour up the visual hierarchy, while it was reduced for achromatic variations, which may offer a useful representation of visual information for perception of natural images.

CRediT authorship contribution statement

Rebecca Lowndes: Writing – review & editing, Writing – original draft, Software, Methodology, Investigation, Formal analysis, Data curation, Conceptualization. **Richard Aveyard:** Software. **Lauren E. Welbourne:** Investigation. **Alex Wade:** Supervision, Software. **Antony B. Morland:** Writing – review & editing, Supervision, Software, Methodology, Investigation, Formal analysis, Conceptualization.

Declaration of Competing Interest

The authors declare that they have no known competing financial interests or personal relationships that could have appeared to influence the work reported in this paper.

Data availability

Data will be made available on request.

Acknowledgments

Supported by funding from BBSRC (BB/P007252).

References

Akaike, H. (1974). A new look at the statistical model identification. *IEEE Transactions on Automatic Control, 19*(6), 716–723.
Albrecht, D. G., & Hamilton, D. B. (1982). Striate cortex of monkey and cat: Contrast response function. *Journal of Neurophysiology, 48*(1), 217–237.
Alvarez, I., De Haas, B. A., Clark, C. A., Rees, G., & Schwarzkopf, D. S. (2015). Comparing different stimulus configurations for population receptive field mapping in human fMRI. *Frontiers in human neuroscience, 9*, 96.
Baker, D. H., Meese, T. S., & Summers, R. J. (2007). Psychophysical evidence for two routes to suppression before binocular summation of signals in human vision. *Neuroscience, 146*(1), 435–448.
Barbur, J. L., Harlow, J., & Plant, G. T. (1994). Insights into the different exploits of colour in the visual cortex. *Proceedings of the Royal Society of London. Series B: Biological Sciences, 258*(1353), 327-334.
Barnett, M. A., Aguirre, G. K., & Brainard, D. (2021). A quadratic model captures the human V1 response to variations in chromatic direction and contrast. *eLife, 10*, e65590.
Benson, N. C., Butt, O. H., Brainard, D. H., & Aguirre, G. K. (2014). Correction of distortion in flattened representations of the cortical surface allows prediction of V1–V3 functional organization from anatomy. *PLoS Computational Biology, 10*(3), e1003538.
Binda, P., Thomas, J. M., Boynton, G. M., & Fine, I. (2013). Minimizing biases in estimating the reorganization of human visual areas with BOLD retinotopic mapping. *Journal of Vision, 13*(7), 13.
Birch, J., Barbur, J. L., & Harlow, A. J. (1992). New method based on random luminance masking for measuring isochromatic zones using high resolution colour displays. *Ophthalmic and Physiological Optics, 12*(2), 133–136.
Bonds, A. B. (1991). Temporal dynamics of contrast gain in single cells of the cat striate cortex. *Visual neuroscience, 6*(3), 239–255.
Bowmaker, J. K., & Dartnall, H. (1980). Visual pigments of rods and cones in a human retina. *The Journal of physiology, 298*(1), 501–511.
Boynton, G. M., Engel, S. A., Glover, G. H., & Heeger, D. J. (1996). Linear systems analysis of functional magnetic resonance imaging in human V1. *Journal of Neuroscience, 16*(13), 4207–4221.
Bradley, A., Zhang, X., & Thibos, L. (1992). Failures of isoluminance caused by ocular chromatic aberrations. *Applied Optics, 31*(19), 3657–3667.
Brown, P. K., & Wald, G. (1964). Visual pigments in single rods and cones of the human retina. *Science, 144*(3614), 45–52.
Buracas, G. T., & Boynton, G. M. (2007). The effect of spatial attention on contrast response functions in human visual cortex. *Journal of Neuroscience, 27*(1), 93–97.
Callaway, E. M., & Wiser, A. K. (1996). Contributions of individual layer 2–5 spiny neurons to local circuits in macaque primary visual cortex. *Visual neuroscience, 13*(5), 907–922.
Carandini, M., & Heeger, D. J. (2012). Normalization as a canonical neural computation. *Nature Reviews Neuroscience, 13*(1), 51–62.
Chatterjee, S., & Callaway, E. M. (2002). S cone contributions to the magnocellular visual pathway in macaque monkey. *Neuron, 35*(6), 1135–1146.
Chen, C.-C., Foley, J. M., & Brainard, D. H. (2000a). Detection of chromoluminance patterns on chromoluminance pedestals I: Threshold measurements. *Vision research, 40*(7), 773–788.
Chen, C.-C., Foley, J. M., & Brainard, D. H. (2000b). Detection of chromoluminance patterns on chromoluminance pedestals II: Model. *Vision Research, 40*(7), 789–803.
Chen, S.-F., Chang, Y., & Wu, J.-C. (2001). The spatial distribution of macular pigment in humans. *Current Eye Research, 23*(6), 422–434.
Conway, B. R. (2009). Color vision, cones, and color-coding in the cortex. *The Neuroscientist, 15*(3), 274–290.
Cornsweet, T. N., & Teller, D. Y. (1965). Relation of increment thresholds to brightness and luminance. *JOSA, 55*(10), 1303–1308.
Dacey, D. M., & Lee, B. B. (1994). The'blue-on'opponent pathway in primate retina originates from a distinct bistratified ganglion cell type. *Nature, 367*(6465), 731–735.
Dale, A. M. (1999). Optimal experimental design for event-related fMRI. *Human Brain Mapping, 8*(2–3), 109–114.
Dale, A. M., Fischl, B., & Sereno, M. I. (1999). Cortical surface-based analysis: I. Segmentation and surface reconstruction. *NeuroImage, 9*(2), 179–194.
Davies, N. P., & Morland, A. B. (2004). Macular pigments: Their characteristics and putative role. *Progress in Retinal and Eye Research, 23*(5), 533–559.
DeAngelis, G. C., Ohzawa, I., & Freeman, R. D. (1993). Spatiotemporal organization of simple-cell receptive fields in the cat's striate cortex. II. Linearity of temporal and spatial summation. *Journal of neurophysiology, 69*(4), 1118–1135.
Derrington, A. M., Krauskopf, J., & Lennie, P. (1984). Chromatic mechanisms in lateral geniculate nucleus of macaque. *The Journal of physiology, 357*(1), 241–265.
Dougherty, R. F., Koch, V. M., Brewer, A. A., Fischer, B., Modersitzki, J., & Wandell, B. A. (2003). Visual field representations and locations of visual areas V1/2/3 in human visual cortex. *Journal of Vision, 3*(10), 1.
Dumoulin, S. O., & Wandell, B. A. (2008). Population receptive field estimates in human visual cortex. *NeuroImage, 39*(2), 647–660.
Engel, S., Zhang, X., & Wandell, B. (1997). Colour tuning in human visual cortex measured with functional magnetic resonance imaging. *Nature, 388*(6637), 68–71.
Eskew, R. T., Jr (2009). Higher order color mechanisms: A critical review. *Vision research, 49*(22), 2686–2704.
Foley, J. M. (1994). Human luminance pattern-vision mechanisms: Masking experiments require a new model. *JOSA A, 11*(6), 1710–1719.
Foley, J. M., & Chen, C.-C. (1997). Analysis of the effect of pattern adaptation on pattern pedestal effects: A two-process model. *Vision research, 37*(19), 2779–2788.
Georgeson, M. A., Wallis, S. A., Meese, T. S., & Baker, D. H. (2016). Contrast and lustre: A model that accounts for eleven different forms of contrast discrimination in binocular vision. *Vision Research, 129*, 98–118.
Glasser, M. F., Sotiropoulos, S. N., Wilson, J. A., Coalson, T. S., Fischl, B., Andersson, J. L., Xu, J., Jbabdi, S., Webster, M., & Polimeni, J. R. (2013). The minimal preprocessing pipelines for the Human Connectome Project. *NeuroImage, 80*, 105–124.
Goodchild, A. K., Ghosh, K. K., & Martin, P. R. (1996). Comparison of photoreceptor spatial density and ganglion cell morphology in the retina of human, macaque monkey, cat, and the marmoset Callithrix jacchus. *Journal of Comparative Neurology, 366*(1), 55–75.
Gouws, A. D., Alvarez, I., Watson, D. M., Uesaki, M., Rogers, J., & Morland, A. B. (2014). On the role of suppression in spatial attention: Evidence from negative BOLD in human subcortical and cortical structures. *Journal of Neuroscience, 34*(31), 10347–10360.
Hammond, B. R., Wooten, B. R., & Snodderly, D. M. (1997). Individual variations in the spatial profile of human macular pigment. *JOSA A, 14*(6), 1187–1196.
Heeger, D. J. (1992). Normalization of cell responses in cat striate cortex. *Visual Neuroscience, 9*(2), 181–197.
Hupé, J.-M., Bordier, C., & Dojat, M. (2012). A BOLD signature of eyeblinks in the visual cortex. *NeuroImage, 61*(1), 149–161.

Jenkinson, M., Bannister, P., Brady, M., & Smith, S. (2002). Improved optimization for the robust and accurate linear registration and motion correction of brain images. *NeuroImage, 17*(2), 825–841.
Jenkinson, M., & Smith, S. (2001). A global optimisation method for robust affine registration of brain images. *Medical image analysis, 5*(2), 143–156.
Johnson, E. N., Hawken, M. J., & Shapley, R. (2008). The orientation selectivity of color-responsive neurons in macaque V1. *Journal of Neuroscience, 28*(32), 8096–8106.
Li, X., Chen, Y., Lashgari, R., Bereshpolova, Y., Swadlow, H. A., Lee, B. B., & Alonso, J. M. (2015). Mixing of chromatic and luminance retinal signals in primate area V1. *Cerebral Cortex, 25*(7), 1920–1937.
Liu, J., & Wandell, B. A. (2005). Specializations for chromatic and temporal signals in human visual cortex. *Journal of Neuroscience, 25*(13), 3459–3468.
Livingstone, M., & Hubel, D. (1988). Segregation of form, color, movement, and depth: Anatomy, physiology, and perception. *Science, 240*(4853), 740–749.
Logothetis, N. K., Pauls, J., Augath, M., Trinath, T., & Oeltermann, A. (2001). Neurophysiological investigation of the basis of the fMRI signal. *Nature, 412*(6843), 150–157.
Lowndes, R., Welbourne, L., Williams, M., Gouws, A., Wade, A., & Morland, A. (2023). Increasing spatial frequency of S-cone defined gratings reduces their visibility and brain response more than for gratings defined by LM cone contrast. *Vision Research, 207*, Article 108209.
Martinovic, J. (2014). *Magno-, Parvo-,Koniocellular Pathways. Encyclopedia of Color Science and Technology* (pp. 1–5). Berlin, Heidelberg: Springer.
Martinovic, J., & Andersen, S. K. (2018). Cortical summation and attentional modulation of combined chromatic and luminance signals. *NeuroImage, 176*, 390–403.
Medina, J. M., & Mullen, K. T. (2009). Cross-orientation masking in human color vision. *Journal of Vision, 9*(3), 20.
Meese, T. S., & Holmes, D. J. (2010). Orientation masking and cross-orientation suppression (XOS): Implications for estimates of filter bandwidth. *Journal of Vision, 10*(12), 9.
Mullen, K. T., Dumoulin, S. O., McMahon, K. L., De Zubicaray, G. I., & Hess, R. F. (2007). Selectivity of human retinotopic visual cortex to S-cone-opponent, L/M-cone-opponent and achromatic stimulation. *European Journal of Neuroscience, 25*(2), 491–502.
Mullen, K. T., Kim, Y. J., & Gheiratmand, M. (2014). Contrast normalization in colour vision: The effect of luminance contrast on colour contrast detection. *Scientific Reports, 4*(1), 7350.
Murasugi, C. M., & Cavanagh, P. (1988). Anisotropy in the chromatic channel: A horizontal-vertical. *Spatial Vision, 3*(4), 281–291.
Nestares, O., & Heeger, D. J. (2000). Robust multiresolution alignment of MRI brain volumes. *Magnetic Resonance in Medicine: An Official Journal of the International Society for Magnetic Resonance in Medicine, 43*(5), 705–715.
Ohzawa, I., Sclar, G., & Freeman, R. D. (1982). Contrast gain control in the cat visual cortex. *Nature, 298*(5871), 266–268.
Ohzawa, I., Sclar, G., & Freeman, R. D. (1985). Contrast gain control in the cat's visual system. *Journal of neurophysiology, 54*(3), 651–667.
Petrov, Y., Carandini, M., & McKee, S. (2005). Two distinct mechanisms of suppression in human vision. *Journal of Neuroscience, 25*(38), 8704–8707.
Rahimi-Nasrabadi, H., Jin, J., Mazade, R., Pons, C., Najafian, S., & Alonso, J.-M. (2021). Image luminance changes contrast sensitivity in visual cortex. *Cell Reports, 34*(5), Article 108692.
Reuter, M., Schmansky, N. J., Rosas, H. D., & Fischl, B. (2012). Within-subject template estimation for unbiased longitudinal image analysis. *NeuroImage, 61*(4), 1402–1418.
Ruddock, K. H. (1963). Evidence for macular pigmentation from colour matching data. *Vision Research, 3*(9–10), 417–429.
Shapley, R., & Hawken, M. J. (2011). Color in the cortex: Single-and double-opponent cells. *Vision Research, 51*(7), 701–717.
Sincich, L. C., & Horton, J. C. (2005). The circuitry of V1 and V2: Integration of color, form, and motion. *Annual Review of Neuroscience, 28*, 303–326.
Smith, S. M., Jenkinson, M., Woolrich, M. W., Beckmann, C. F., Behrens, T. E. J., Johansen-Berg, H., Bannister, P. R., De Luca, M., Drobnjak, I., & Flitney, D. E. (2004). Advances in functional and structural MR image analysis and implementation as FSL. *NeuroImage, 23*, S208–S219.
Smith, V. C., & Pokorny, J. (1975). Spectral sensitivity of the foveal cone photopigments between 400 and 500 nm. *Vision Research, 15*(2), 161–171.
Snodderly, D. M., Auran, J. D., & Delori, F. C. (1984). The macular pigment. II. Spatial distribution in primate retinas. *Investigative Ophthalmology & Visual Science, 25*(6), 674–685.
Solomon, S. G., & Lennie, P. (2005). Chromatic gain controls in visual cortical neurons. *Journal of Neuroscience, 25*(19), 4779–4792.
Srinivasan, V. J., Monson, B. K., Wojtkowski, M., Bilonick, R. A., Gorczynska, I., Chen, R., Duker, J. S., Schuman, J. S., & Fujimoto, J. G. (2008). Characterization of outer retinal morphology with high-speed, ultrahigh-resolution optical coherence tomography. *Investigative Ophthalmology & Visual Science, 49*(4), 1571–1579.
Stockman, A., & Sharpe, L. T. (2000). Tritanopic color matches and the middle-and long-wavelength-sensitive cone spectral sensitivities. *Vision Research, 40*(13), 1739–1750.
Strasburger, H., Bach, M., & Heinrich, S. P. (2018). Blur unblurred—a mini tutorial. *i-Perception, 9*(2), 2041669518765850.
Sun, H., Smithson, H. E., Zaidi, Q., & Lee, B. B. (2006). Do magnocellular and parvocellular ganglion cells avoid short-wavelength cone input? *Visual Neuroscience, 23*(3–4), 441–446.
Tregillus, K. E. M., Isherwood, Z. J., Vanston, J. E., Engel, S. A., MacLeod, D. I. A., Kuriki, I., & Webster, M. A. (2021). Color compensation in anomalous trichromats assessed with fMRI. *Current Biology, 31*(5), 936–942.
Van Essen, D. C., & Gallant, J. L. (1994). Neural mechanisms of form and motion processing in the primate visual system. *Neuron, 13*(1), 1–10.
Vernon, R. J. W., Gouws, A. D., Lawrence, S. J. D., Wade, A. R., & Morland, A. B. (2016). Multivariate patterns in the human object-processing pathway reveal a shift from retinotopic to shape curvature representations in lateral occipital areas, LO-1 and LO-2. *Journal of Neuroscience, 36*(21), 5763–5774.
Wandell, B. A., Dumoulin, S. O., & Brewer, A. A. (2006). Computational neuroimaging: Color signals in the visual pathways. *Neuro-Ophthalmology, 23*, 324–343.
Wang, Z., Bovik, A. C., Sheikh, H. R., & Simoncelli, E. P. (2004). Image quality assessment: From error visibility to structural similarity. *IEEE Transactions on Image Processing, 13*(4), 600–612.
Welbourne, L. E., Morland, A. B., & Wade, A. R. (2018). Population receptive field (pRF) measurements of chromatic responses in human visual cortex using fMRI. *NeuroImage, 167*, 84–94.
Woolrich, M. W., Ripley, B. D., Brady, M., & Smith, S. M. (2001). Temporal autocorrelation in univariate linear modeling of FMRI data. *NeuroImage, 14*(6), 1370–1386.